arXiv:1806.06402v1 [cond-mat.mes-hall] 17 Jun 2018

Interactions and magnetotransport through spin-valley coupled Landau levels in monolayer MoS_2

Riccardo Pisoni[1*], Andor Kormányos[2], Matthew Brooks[2], Zijin Lei[1], Patrick Back[3], Marius Eich[1], Hiske Overweg[1], Yongjin Lee[1], Peter Rickhaus[1], Kenji Watanabe[4], Takashi Taniguchi[4], Atac Imamoglu[3], Guido Burkard[2], Thomas Ihn[1] and Klaus Ensslin[1*].

[1] *Solid State Physics Laboratory, Department of Physics, ETH Zürich, 8093 Zürich, Switzerland*

[2] *Department of Physics, University of Konstanz, D-78464 Konstanz, Germany*

[3] *Institute of Quantum Electronics, Department of Physics, ETH Zürich, 8093 Zürich, Switzerland*

[4] *National Institute for Material Science, 1-1 Namiki, Tsukuba 305-0044, Japan*

[*] *E-mails: pisonir@phys.ethz.ch; ensslin@phys.ethz.ch*

The strong spin-orbit coupling and the broken inversion symmetry in monolayer transition metal dichalcogenides (TMDs) results in spin-valley coupled band structures. Such a band structure leads to novel applications in the fields of electronics and optoelectronics. Density functional theory calculations as well as optical experiments have focused on spin-valley coupling in the valence band. Here we present magnetotransport experiments on high-quality n-type monolayer molybdenum disulphide (MoS_2) samples, displaying highly resolved Shubnikov-de Haas oscillations at magnetic fields as low as $2\,\mathrm{T}$. We find the effective mass $0.7\,\mathrm{m_e}$, about twice as large as theoretically predicted and almost independent of magnetic field and carrier density. We further detect the occupation of the second spin-orbit split band at an energy of about $15\,\mathrm{meV}$, i.e. about a factor 5 larger than predicted.[1–3] In ad-

dition, we demonstrate an intricate Landau level spectrum arising from a complex interplay between a density-dependent Zeeman splitting and spin and valley-split Landau levels. These observations, enabled by the high electronic quality of our samples, testify to the importance of interaction effects in the conduction band of monolayer MoS_2.

Monolayer transition metal dichalcogenides (TMDs) such as MoS_2, $MoSe_2$, WS_2 and WSe_2 are two-dimensional (2D) semiconductors with band extrema at the corners (K, K′-points) of the first Brillouin zone.[4] Due to the strong spin-orbit coupling the spin degeneracy in the K and K′ valleys is lifted, with opposite spin polarization normal to the layer plane in opposite valleys (see Figure 2, inset). This peculiar band structure with coupled spin and valley degrees of freedom results in an anomalous Landau level (LL) structure.[5,6] Theoretical proposals predict the formation of LLs under the influence of a perpendicular magnetic field that are arranged differently from those in conventional semiconductor quantum wells and graphene.[6] Magnetotransport measurements have recently been performed in monolayer WSe_2, $MoSe_2$ and bilayer MoS_2 revealing two-fold degenerate LLs, large effective masses and carrier density dependent Zeeman splitting.[7–11]

Here we report transport measurements in high mobility dual-gated monolayer MoS_2 under a perpendicular magnetic field. Shubnikov-de Haas (SdH) oscillations appear at magnetic fields as low as $B \approx 2\,\mathrm{T}$ at a temperature of $T \approx 100\,\mathrm{mK}$. From the temperature dependence of the SdH oscillations we measure an electron effective mass of $\approx 0.7\,\mathrm{m_e}$, compared to a value of $0.4\,\mathrm{m_e}$ predicted by Density Functional Theory (DFT) calculations.[1–3,12] By increasing the electron density, we observe an interplay between even and odd filling factor sequences explained qualitatively

by a density-dependent effective g-factor, similar to observations in p-doped WSe_2 and n-doped $MoSe_2$ monolayers.[8,10]. At electron densities $> 4 \times 10^{12}\,\mathrm{cm}^{-2}$, corresponding to a Fermi energy $> 15\,\mathrm{meV}$, the upper spin-orbit split bands start to be populated and the complex LL structure of the different valley-spin polarized bands is observed.

High mobility TMD field effect devices were fabricated using a van der Waals heterostructure platform.[13,14] A schematic of the device is shown in Figure 1a. Monolayer MoS_2 flakes were encapsulated between two hexagonal boron nitride (hBN) layers and graphite flakes serve as top and bottom gates. We fabricated and measured four monolayer MoS_2 samples, labelled A, B, C and D, which show consistent behaviour. We will mainly discuss sample A here. Data from samples B, C and D are presented in the Supplementary. Figure 1b shows the optical micrograph of sample A with the MoS_2 flake outlined in black. The inset of Figure 1b displays a sketch of the MoS_2 flake where the ohmic contacts are numbered from 1 to 4. Contacts 2 and 4 are used for current injection and extraction, contacts 1 and 3 serve as voltage probes. The top and bottom hBN outlined in cyan and blue, respectively, serve as dielectric layers to insulate the conducting MoS_2 from the top and bottom graphite gates. We use graphite as a gate electrode because it provides an atomically flat surface and a uniform potential landscape for the MoS_2 layer.[13,15,16]

The high electron mobility and low contact resistances allow us to investigate quantum transport phenomena in single-layer MoS_2 using standard lock-in techniques at $31.4\,\mathrm{Hz}$. All measurements presented here are performed at $V_{\mathrm{TG}} = 8\,\mathrm{V}$ in order to ensure Ohmic behaviour of the contacts at low temperatures. In Figure 1c we present the four terminal resistance $R_{24,13}$ as a func-

tion of magnetic field B at $V_{\mathrm{BG}} = -2.2\,\mathrm{V}$, $n_{\mathrm{SdH}} \approx 2.9 \times 10^{12}\ \mathrm{cm}^{-2}$, and $T \approx 100\,\mathrm{mK}$ (left vertical dashed line in Figure 2). SdH oscillations start at $B \approx 2\,\mathrm{T}$ yielding a lower bound for the quantum mobility of $\approx 5,000\ \mathrm{cm}^2/\mathrm{Vs}$. The electron density is determined from the SdH oscillations according to $n_{\mathrm{SdH}} = (e/h)(1/\Delta(1/B))$, where $\Delta(1/B)$ is the period of the SdH oscillations in $1/B$. At $n_{\mathrm{SdH}} \approx 2.9 \times 10^{12}\ \mathrm{cm}^{-2}$ we measure an alternating sequence of deeper and shallower minima corresponding to odd and even filling factors, respectively, meaning that the Landau levels of the K and K′ valleys are no longer degenerate. The inset of Figure 1c displays the $I - V_{\mathrm{bias}}$ traces as a function of V_{TG} at $V_{\mathrm{BG}} = 0\,\mathrm{V}$ and $T \approx 100\,\mathrm{mK}$. The linearity of the $I - V_{\mathrm{bias}}$ curves for $V_{\mathrm{TG}} > 2\,\mathrm{V}$ indicates the regime of a good ohmic contact at low temperatures.

In order to determine the effective mass we measure in Figure 1d the four-terminal resistance $\Delta R_{24,13}$ with a smooth background subtracted as a function of B at various elevated temperatures ranging from $1.7\,\mathrm{to}\ 4.5\,\mathrm{K}$ at $V_{\mathrm{BG}} = -1.5\,\mathrm{V}$, $n_{\mathrm{SdH}} \approx 4.1 \times 10^{12}\ \mathrm{cm}^{-2}$ (right vertical dashed line in Figure 2). We observe the sequence of even filling factors $\nu = 22,\ 24,\ 26,\ 28$ since the splitting of the K and K′ valleys is not resolved for these elevated temperatures. From the T-dependence of the SdH oscillation amplitudes we extract the electron effective mass m^* by fitting $\Delta R_{24,13}$ to $x/sinh(x)$, where $x = 2\pi^2 k_B T/\hbar\omega_c$ and $\omega_c = eB/m^*$ is the cyclotron frequency (see Supplementary).[17,18] In the inset of Figure 1d we present m^* at various electron densities n_{SdH} for the four different samples. For samples A and C we calculate the density-averaged mass $m^*/m_e = 0.65 \pm 0.04$ where m_e is the electron rest mass. For sample B, $m^*/m_e = 0.75 \pm 0.03$. Sample D shows $0.7 \leq m^*/m_e \leq 0.8$ with larger error bars compared to the other three samples due to a less precise temperature calibration. No obvious dependence of the mass on n_{SdH} or B is

observed. These m^* values are larger than those of DFT studies which predict $m^*/m_e \approx 0.4$ for single layer MoS_2.[1–3, 12]

In Figure 2 we present an overview of the four-terminal magneto-resistance $R_{24,13}$ (color scale) over a wide range of V_{BG} and B applied perpendicularly to the sample at $T \approx 100\,\mathrm{mK}$. There are three qualitatively different regions which we discuss in the following. The first region (I) corresponds to $V_{\mathrm{BG}} < -1.6\,\mathrm{V}$, the second region (II) to $-1.6\,\mathrm{V} < V_{\mathrm{BG}} < 1\,\mathrm{V}$ and the third region (III) to $V_{\mathrm{BG}} > 1\,\mathrm{V}$. The black dashed lines in the inset of Figure 1c indicate the Fermi energies corresponding to regions (I), (II) and (III).

We now discuss region (I) of the Landau fan diagram shown in Figure 2. Figure 3a shows a blow-up of the four-terminal resistance $R_{24,31}$ in this region as a function of V_{BG} and B at $T \approx 100\,\mathrm{mK}$. We observe two sets of LLs with different amplitudes that we attribute to the valley K spin-down and K′ spin-up LLs. In Figure 3b, c, d we show the SdH oscillations for three representative electron densities. Both for $n_{SdH} = 2.4 \times 10^{12}\ \mathrm{cm}^{-2}$ (Figure 3b) and $n_{SdH} = 3.8 \times 10^{12}\ \mathrm{cm}^{-2}$ (Figure 3d) one can observe an alternating sequence of deeper (primary) and shallower (secondary) minima. While for the lower density the primary minima are at odd filling factors ν, for the higher density they are at even ν. For the transition density $n_{SdH} = 3.1 \times 10^{12}\ \mathrm{cm}^{-2}$ (Figure 3c) the minima at even and odd filling factors are approximately equally deep. This means that by tuning the electron density we observe a transition from a predominantly odd to a predominantly even filling factor sequence.

For the considered electron densities electron-electron interactions are expected to play a

significant role[8,10], similar to other multi-valley two-dimensional systems[19–21]. The interaction strength can be characterized by the dimensionless Wigner-Seitz radius $r_s = 1/(\sqrt{\pi\, n_{\rm e}} a_{\rm B}^*)$, where $a_{\rm B}^* = a_{\rm B}(\kappa m_{\rm e}/m^*)$ is the effective Bohr radius, κ the dielectric constant and $a_{\rm B}$ the Bohr radius. For the regime $-3.2\,{\rm V} < V_{\rm BG} < -1.6\,{\rm V}$ we estimate that $r_s = 9.8 - 7.5$, placing the system in a regime where interactions are important. Qualitatively, the observations can be explained by an extended single particle picture, where electron-electron interaction effects are accounted for by assuming i) $n_{\rm SdH}$-*dependent* valley g-factor $g_{\rm vl}$, and ii) in good approximation $n_{\rm SdH}$-*independent* effective mass m^*.

For data taken at $1.7\,{\rm K}$ there are regimes where only even or odd filling factors are visible (see Supplementary). A model suggested in the literature[8,10] based on a density dependent g-factor is in good agreement with these data (see Supplementary). Such a model will necessarily lead to a situation where neighbouring Landau levels become accidentally degenerate and the corresponding SdH minimum will disappear. Our low temperature data shown in Figure 3b, c, d indicate however, that neighbouring Landau levels are never degenerate, demonstrating the limitations of such a simple model. Extreme cases of such anti-crossings at $T \approx 100\,{\rm mK}$ are indicated with white circles in Figure 3a. These anticrossings, which happen for approximately integer value of the ratio of valley Zeeman energy with respect to cyclotron energy E_{vz}/E_c, cannot be explained in a single particle picture where the LLs in the K and K′ valleys are assumed to have out-of-plane (i.e., parallel to the magnetic field) and orthogonal spin-polarization, since this would imply that they should cross. Instead, these anticrossings can arise as a result of electron-electron interaction effects, that mix single-particle LLs of opposite spin and lead to not fully spin polarized LLs.

Continuing with region (II) in Figure 2, at $V_{\mathrm{BG}} = -1.6\,\mathrm{V}$, $n_{\mathrm{SdH}} \approx 4\times10^{12}\,\mathrm{cm}^{-2}$ (black arrow), we observe two important changes in the SdH oscillations. First, as shown in the Supplementary, there is another even to odd transition in the SdH oscillation minima like in region (I) with the same interpretation. Second, as indicated in Figure 2 with cyan dashed lines [one in region (I), the other in region (III)], there is a sudden change in the slope of the SdH minima related to constant filling factor by about a factor of two in the Landau fan diagram at the left edge of region (II). A factor of two is expected when the density of states doubles. The Hall mobility μ and the four terminal resistance $R_{24,13}$ at zero magnetic field exhibit a pronounced change in slope at the same point (Supplementary). We attribute these observations to the occupation of the upper spin-orbit split K and K′ valleys in the conduction band of monolayer MoS_2 , as sketched in the inset of Figure 1c.

A zoom into region (II) is shown in Figure 4a. As we show in the inset of Figure 4a, the difference between the total electron density (black dashed line) and that of the lower spin-orbit split bands (blue circles) increases linearly as a function of V_{BG} for $n_{\mathrm{SdH}} \approx 4\times10^{12}\,\mathrm{cm}^{-2}$. The "missing" electron density (green circles) leads to a calculated additional Landau fan (green dashed lines in Figure 3a) which is compatible with the appearance of the intermittent shifts of the SdH maxima in this region.

The threshold electron density where the slope change occurs is $n_{\mathrm{SdH}} \approx 4\times10^{12}\,\mathrm{cm}^{-2}$. Assuming a 2D density of states $DOS = m^*/\pi\hbar^2$ implying a two-fold degeneracy and using the experimentally determined effective mass, we calculate the Fermi energy to be $E_F \approx 15\,\mathrm{meV}$,

which gives us an estimate of the intrinsic spin-orbit interaction $2\Delta^*_{cb}$ for K-valley electrons in monolayer MoS_2. This value of $2\Delta^*_{cb}$ is about a factor of five larger than the results of DFT band structure calculations[1]. We note that a similar (albeit smaller) enhancement of $2\Delta^*_{cb}$ with respect to theoretical calculations was also observed[10] for monolayer $MoSe_2$. This apparent enhancement of the spin splitting of the bands might be due to an exchange interaction driven band renormalization. Although the upper spin-orbit split bands start to be filled, we found that, at $T \approx 1.7\,\mathrm{K}$ the measurements can still be fitted nicely (see Supplementary) assuming that only the lower spin-orbit split bands give visible contributions to the SdH oscillations. The effect of the LLs corresponding to the upper spin-orbit split bands become apparent at lower temperatures where the distinctive "wavyness" of the bright lines (Figure 4a) suggests that LLs corresponding to the lower spin-orbit split bands are affected by the LLs originating from the upper spin-orbit split bands.

We also note that, as shown in the Supplementary, photoluminescence measurements exhibit, at $n_{\mathrm{SdH}} \approx 4 \times 10^{12}\ \mathrm{cm}^{-2}$, a third peak, at lower energy than that of the exciton and the attractive polaron[22] peaks, indicating the emergence of a new emission channel. We speculate that this emission channel is linked to the formation of a dark polaron state where an intra-valley dark exciton state is dynamically screened by electrons with opposite spin from the same valley. As the Fermi energy E_{F} crosses over to the spin-orbit split band at E_{SO}, the spin-dark intra-valley exciton becomes stable and has a lower energy than the bright exciton: this is a conseqence of the fact that the dark exciton is not subject to electron-hole exchange induced blue shift. Moreover, in contrast to the bright exciton, the dark exciton is not subject to phase-space filling for $E_{\mathrm{F}} \approx E_{\mathrm{SO}}$, further reducing its binding energy. Photoluminescence of dark polaron should take place at a finite but

reduced rate due to radiative recombination of the valence hole and an electron from the screening cloud. Time resolved measurements determining the lifetime of the new emission peak can be used to verify this explanation.

Figure 4b shows a zoom-in of Figure 2 for region (III) at $T \approx 100\,\mathrm{mK}$. We observe the appearance of anticrossings, a signature of split spin-valley coupled LLs originating from the lower and upper spin-orbit split bands. These observations indicate again that a standard single particle picture for the description of Landau levels is insufficient. It is remarkable that the observed anticrossings seem independent of which spin or/and valley states are involved. No obvious selection rules can be observed. Experimentally we find that the level anti-crossings at a magnetic field of $6\,\mathrm{T}$ can be resolved below a temperature of about $500\,\mathrm{mK}$. This corresponds to an estimated interaction energy scale of $4k_\mathrm{B}T \approx 170\,\mu\mathrm{eV}$. In comparison the single-particle LL splitting $\hbar\omega_\mathrm{c}$ calculated with an effective mass of $0.65\,\mathrm{m_e}$ at $6\,\mathrm{T}$ is $1\,\mathrm{meV}$. We see that the interaction energy is a significant fraction of the Landau level spacing. The disorder-limited energy resolution for LL energy gaps in our experiment must be well below the estimated interaction energy. This in turn is in rough agreement with the quantum mobility of $5,000\ \mathrm{cm^2/Vs}$, which leads to an upper bound for the characteristic disorder energy of $180\,\mu\mathrm{eV}$ if we assume the experimentally deduced effective mass of $0.65\,\mathrm{m_e}$.

Compared to standard semiconductor 2D electron gases such as those in high-mobility AlGaAs heterostructures, where most effects can be quantitatively explained within a single particle-model with the inclusion of exchange effects for small odd filling factors, the data presented here

indicates that the formation of Landau levels in monolayer MoS_2 is governed if not dictated by the combination of both spin-orbit and carrier-carrier interactions.

Quantum Hall ferromagnetism[23,24] is relevant for small filling factors (< 5) and it becomes less pronounced for larger filling factors since a possible overall spin/valley polarization decreases. For our experiments we deal with large filling factors (> 20) and the observed anti-crossings appear to be independent of filling factor. We conclude that exchange enhancement of the g-factor which causes quantum Hall ferromagnetism is not relevant here.

In conclusion, we fabricated high mobility dual-gated single layer MoS_2 devices using a van der Waals heterostructure platform with quantum mobilities as high as $\mu \approx 5,000\ \mathrm{cm}^2/\mathrm{Vs}$. The temperature dependence of the SdH oscillations reveals an electron effective mass of $\approx 0.7\,\mathrm{m_e}$. We are able to measure and resolve the LL structure of the lower spin-orbit split K and K′ valleys. At $n_{\mathrm{SdH}} \approx 4 \times 10^{12}\ \mathrm{cm}^{-2}$, we observe the occupation of the upper spin-orbit split K and K′ valleys, thus estimating $2\Delta^*_{cb} \approx 15\,\mathrm{meV}$. At higher electron densities we observe the appearance of multiple sets of LLs originating from the upper and lower spin-orbit split K and K′ valleys. Interaction effects of valley and spin polarized LLs, at elevated temperatures consistent with a density-dependent g-factor, are observed in the experiments. Measurements of the LL structure of monolayer MoS_2 has been hindered to-date by high contact resistances and low sample mobilities. Our results demonstrate the subtle and unconventional conduction band Landau level structure of monolayer MoS_2, where strong spin-orbit interaction meets strong electron-electron interactions. This indicates the presence of rich, novel and so far unpredicted physics possibly beyond that ex-

pected from single-particle considerations. These prospects bear relevance also for related TMD materials, such as $MoSe_2$, WS_2 and WSe_2.

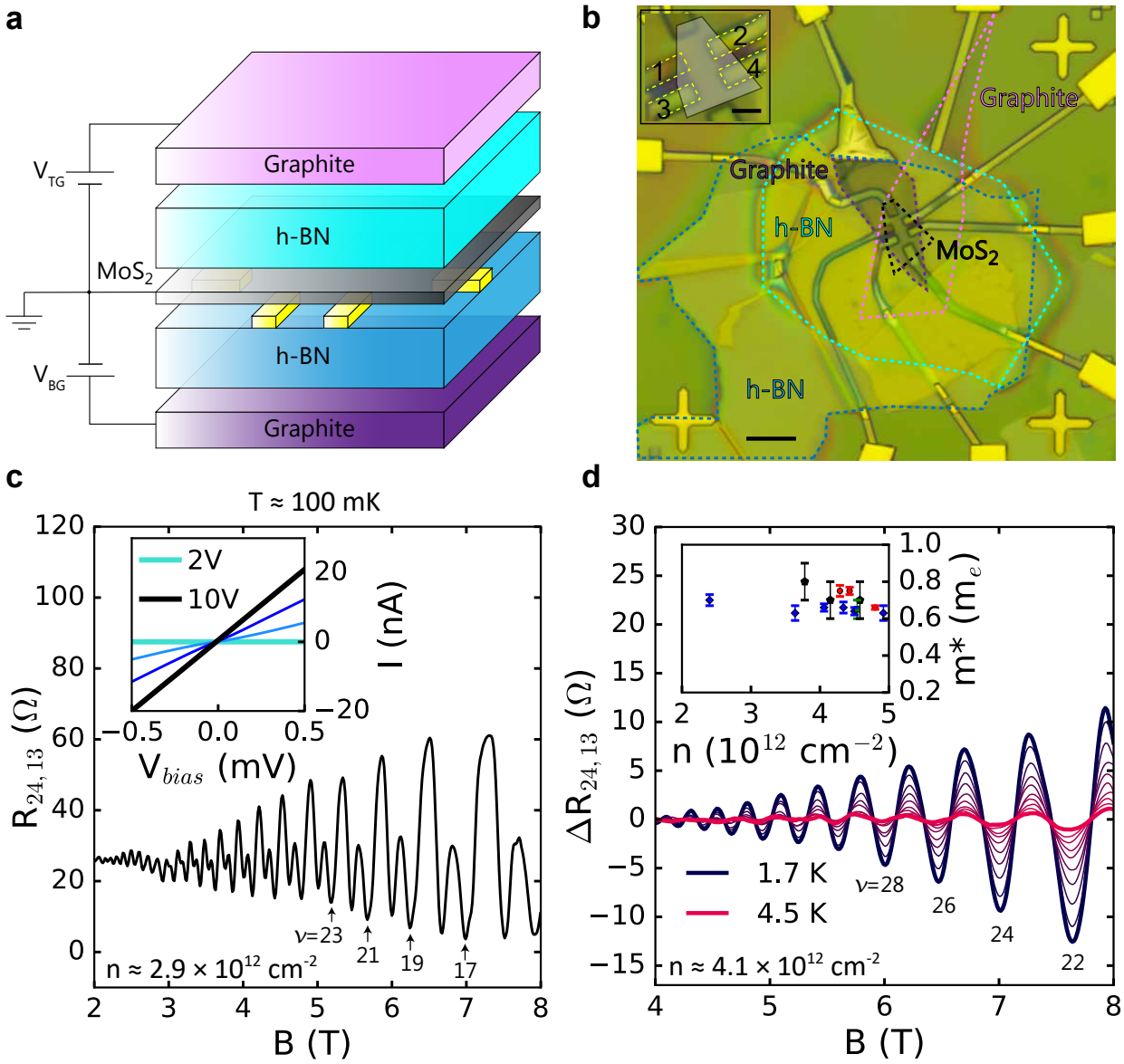

Figure 1 Device structure and electron effective mass in monolayer MoS_2. a, Device schematic. A single layer MoS_2 is encapsulated between two layers of hBN. Graphite flakes are used as bottom and top gates. Ti/Au electrodes are evaporated on top of the bottom hBN before the MoS_2 layer is transferred. **b**, Optical micrograph of the sample. The MoS_2 flake is highlighted with black dashed lines (scale bar is $10\,\mu\mathrm{m}$). Inset: Ti/Au contacts to the MoS_2 flake are numbered 1 - 4 (Scale bar is $2\,\mu\mathrm{m}$). **c**, Four-terminal resistance $R_{24,13}$ as a function of B at $V_{\mathrm{BG}} = -2.2\,\mathrm{V}$, $n_{\mathrm{SdH}} \approx 2.9 \times 10^{12}\ \mathrm{cm}^{-2}$ and $T \approx 100\,\mathrm{mK}$. SdH oscillations appear at $B \approx 2\,\mathrm{T}$. We observe a predominantly odd filling factor sequence $\nu = 17, 19, 21, 23$. Inset: Linear $I - V_{\mathrm{bias}}$ traces as a function of V_{TG} at $T \approx 100\,\mathrm{mK}$. The Ohmic contact regime is achieved for $V_{\mathrm{TG}} > 2\,\mathrm{V}$. **d**, SdH oscillations as a function of the magnetic field for different temperatures at $V_{\mathrm{BG}} = -1.5\,\mathrm{V}$, $n_{\mathrm{SdH}} \approx 4.1 \times 10^{12}\ \mathrm{cm}^{-2}$. An Even filling factor sequence $\nu = 22, 24, 26, 28$ is measured. Inset: effective mass m^* calculated for the four samples as a function of electron density. Blue, red, green and black markers correspond to samples A, B, C and D, respectively.

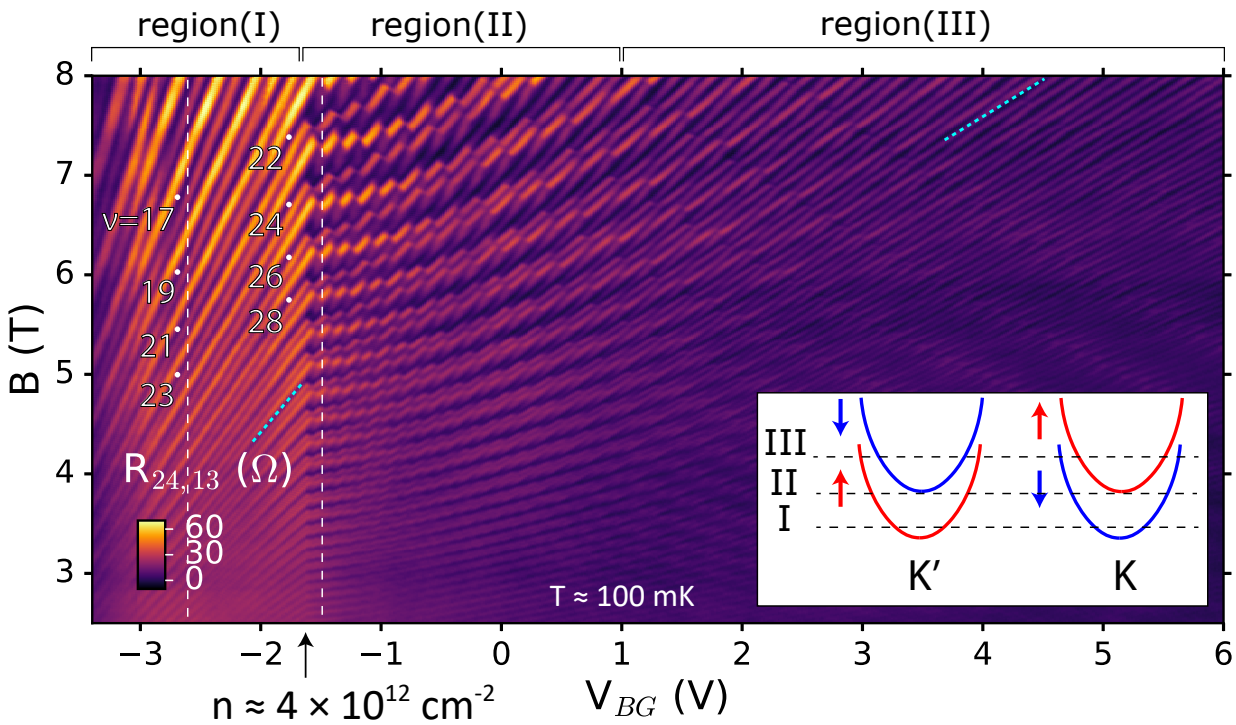

Figure 2 Landau fan diagram of monolayer MoS_2. Four-terminal resistance $R_{24,13}$ as a function of V_{BG} and magnetic field at $T \approx 100\,\mathrm{mK}$. We observe a pronounced change in the slope (cyan dashed lines) of the Landau fan diagram at $V_{\mathrm{BG}} \approx -1.6\,\mathrm{V}$, $n_{\mathrm{SdH}} \approx 4 \times 10^{12}\,\mathrm{cm}^{-2}$ (black arrow). The Landau fan diagram can be divided in three different regions: (I) $V_{\mathrm{BG}} < -1.6\,\mathrm{V}$; (II) $-1.6\,\mathrm{V} < V_{\mathrm{BG}} < 1\,\mathrm{V}$; (III) $V_{\mathrm{BG}} > 1\,\mathrm{V}$. Left and right white dashed lines correspond to the line cuts presented in Figure 1c and Figure 1d, respectively. Inset: Sketch of the conduction band minima at the K and K′ points in the first Brillouin zone of monolayer MoS_2. Due to the strong spin-orbit interaction the spin degeneracy is lifted and spin and valley degrees of freedom are locked. Black dashed lines represent the Fermi energy corresponding to regions (I), (II) and (III), respectively.

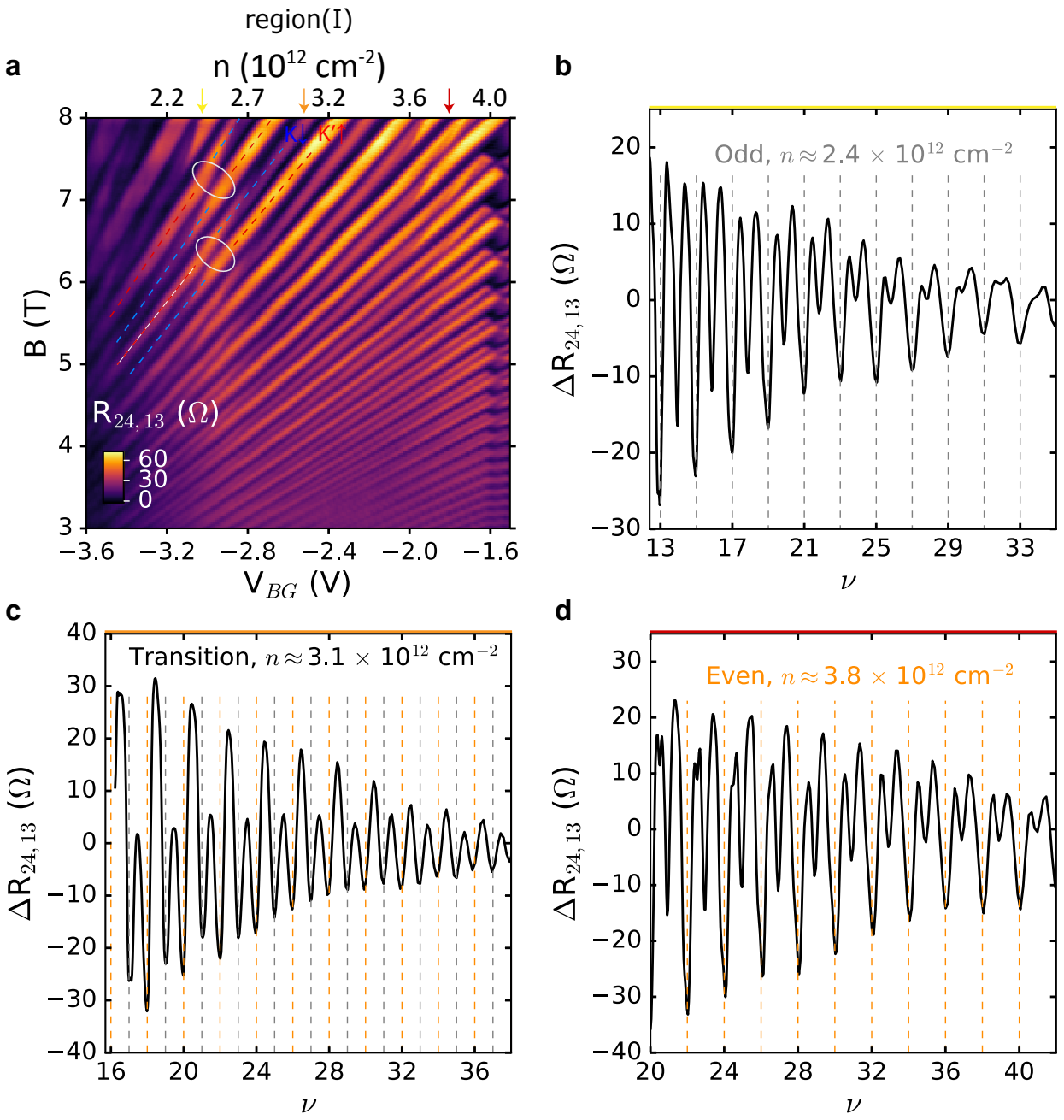
region(I)
a
n (10^{12} cm^{-2})
2.2
2.7
3.2
3.6
4.0
K1
K1'
B (T)
$R_{24,13}$ (Ω)
60
30
0
V_{BG} (V)
b
Odd, $n \approx 2.4 \times 10^{12}$ cm^{-2}
$\Delta R_{24,13}$ (Ω)
ν
c
Transition, $n \approx 3.1 \times 10^{12}$ cm^{-2}
$\Delta R_{24,13}$ (Ω)
ν
d
Even, $n \approx 3.8 \times 10^{12}$ cm^{-2}
$\Delta R_{24,13}$ (Ω)
ν

Figure 3 Even and odd Landau level filling factors sequences in monolayer MoS_2. **a**, Region (I). $R_{24,13}$ as a function of electron density n_{SdH} and magnetic field at $T \approx 100\,\mathrm{mK}$. Two sets of LLs corresponding to the K spin-down and K′ spin-up valleys can be distinguished (blue and red dashed lines, respectively). Anticrossings between not fully spin polarized LLs appear (white circles). **b**, **c**, **d**, Four terminal resistance $\Delta R_{24,13}$, after subtracting a smooth background, as a function of LL filling factors at different electron densities. By increasing the electron density we observe an interplay between predominantly odd and predominantly even filling factors sequences (yellow, orange and red arrows in **a**, respectively).

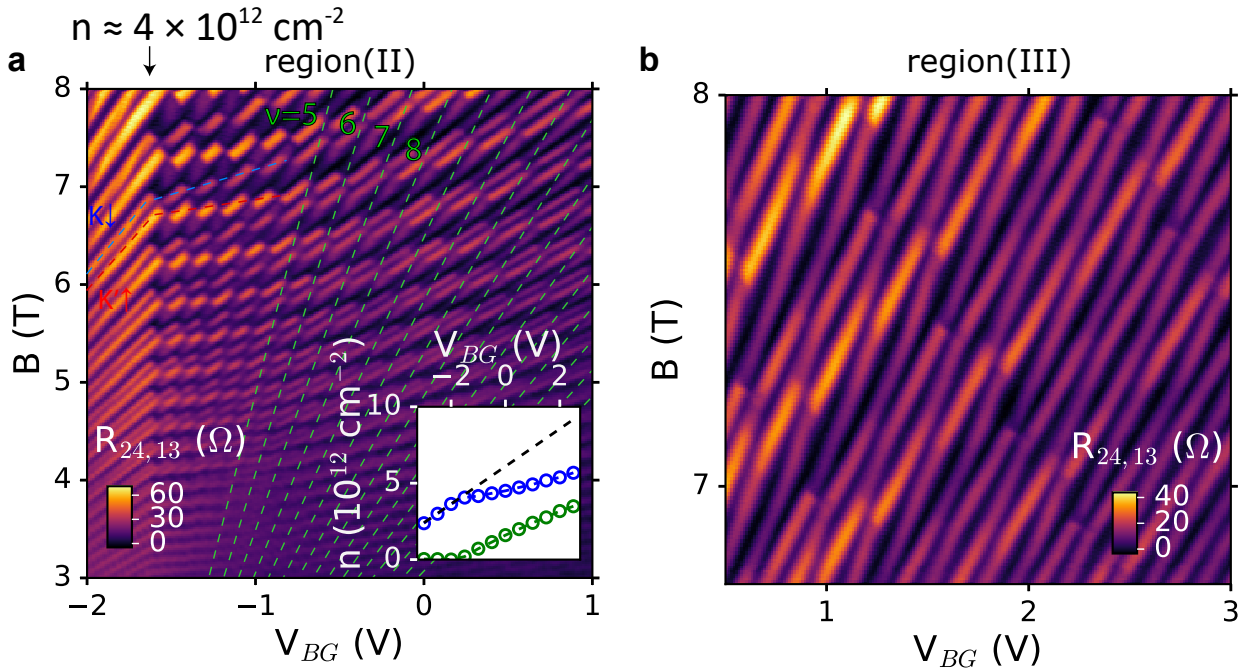

Figure 4 Interaction effects in the Landau level spectrum of monolayer MoS_2. a, Region (II). $R_{24,13}$, as a function of V_{BG} and magnetic field at $T \approx 100\,\mathrm{mK}$. The "wavyness" of the bright lines indicate that the LLs of the lower spin-orbit split bands are affected by the LLs originating from the upper spin-orbit split bands. Inset: electron density as a function of V_{BG}. Black dashed line indicate the total electron density determined from the capacitor model. Blue and green markers represent the lower and upper spin-orbit split bands electron densities, respectively. Green dashed lines in Figure 3**a** indicate the Landau fan diagram originating from the upper spin-orbit split bands. **b**, Region (III). $R_{24,13}$ as a function of V_{BG} and magnetic field at $T \approx 100\,\mathrm{mK}$. Multiple anticrossings through spin-valley coupled LLs are observed.

Methods

The monolayer MoS_2 flakes were exfoliated from a natural bulk crystal (SPI supplies) and identified by optical contrast, atomic force microscopy and photoluminescence characterizations. The exfoliation of the MoS_2 crystal and the assembling of the heterostructure were performed in an argon environment (H_2O and O_2 levels $< 0.1\,\mathrm{ppm}$) in order to prevent the degradation and contamination of the MoS_2 monolayers.[13,14] To assemble the heterostructure we make use of a dry pick-up and transfer technique with a polycarbonate film supported by polydimethylsiloxane.[13,15,25] Gate and contact leads (Ti/Au $10\,\mathrm{nm}/20\,\mathrm{nm}$) were deposited by means of electron-beam (e-beam) evaporation at a pressure of $\approx 10^{-8}\,\mathrm{mbar}$ on top of the bottom hBN and graphite before the transfer of the MoS_2 layer. This fabrication process prevents the MoS_2 flake to be exposed to air, solvents and standard nanofabrication procedures such as e-beam lithography that could affect the quality of the MoS_2 crystal. More details about the fabrication process are provided in the Supplementary.

1. Kormányos, A., Zólyomi, V., Drummond, N. D. & Burkard, G. Spin-Orbit Coupling, Quantum Dots, and Qubits in Monolayer Transition Metal Dichalcogenides. *Physical Review X* **4**, 011034 (2014). URL `http://link.aps.org/doi/10.1103/PhysRevX.4.011034`.

2. Kormányos, A. *et al.* Monolayer MoS_2: Trigonal warping, the Γ valley, and spin-orbit coupling effects. *Physical Review B* **88**, 045416 (2013). URL `https://link.aps.org/doi/10.1103/PhysRevB.88.045416`.

3. Liu, G.-B., Shan, W.-Y., Yao, Y., Yao, W. & Xiao, D. Three-band tight-binding model for

monolayers of group-VIB transition metal dichalcogenides. *Physical Review B* **88**, 085433 (2013). URL https://link.aps.org/doi/10.1103/PhysRevB.88.085433.

4. Xiao, D., Liu, G.-B., Feng, W., Xu, X. & Yao, W. Coupled Spin and Valley Physics in Monolayers of MoS_2 and Other Group-VI Dichalcogenides. *Physical Review Letters* **108**, 196802 (2012). URL http://link.aps.org/doi/10.1103/PhysRevLett.108.196802.

5. Li, X., Zhang, F. & Niu, Q. Unconventional Quantum Hall Effect and Tunable Spin Hall Effect in Dirac Materials: Application to an Isolated MoS_2 Trilayer. *Physical Review Letters* **110**, 066803 (2013). URL https://link.aps.org/doi/10.1103/PhysRevLett.110.066803.

6. Wang, Z., Shan, J. & Mak, K. F. Valley- and spin-polarized Landau levels in monolayer WSe_2. *Nature Nanotechnology* **12**, 144–149 (2017). URL https://www.nature.com/articles/nnano.2016.213.

7. Fallahazad, B. *et al.* Shubnikov-de Haas Oscillations of High-Mobility Holes in Monolayer and Bilayer WSe_2: Landau Level Degeneracy, Effective Mass, and Negative Compressibility. *Physical Review Letters* **116**, 086601 (2016). URL https://link.aps.org/doi/10.1103/PhysRevLett.116.086601.

8. Movva, H. C. *et al.* Density-Dependent Quantum Hall States and Zeeman Splitting in Monolayer and Bilayer WSe_2. *Physical Review Letters* **118**, 247701 (2017). URL https://link.aps.org/doi/10.1103/PhysRevLett.118.247701.

9. Gustafsson, M. V. *et al.* Ambipolar Landau levels and strong band-selective carrier interactions in monolayer WSe_2. *Nature Materials* **17**, 411–415 (2018). URL https://www.nature.com/articles/s41563-018-0036-2.

10. Larentis, S. *et al.* Large effective mass and interaction-enhanced Zeeman splitting of k-valley electrons in $MoSe_2$. *Physical Review B* **97**, 201407 (2018). URL https://link.aps.org/doi/10.1103/PhysRevB.97.201407.

11. Lin, J. *et al.* Probing Landau levels of strongly interacting massive Dirac electrons in layer-polarized MoS_2. *arXiv:1803.08007 [cond-mat]* (2018). URL http://arxiv.org/abs/1803.08007. ArXiv: 1803.08007.

12. Wang, Q. H., Kalantar-Zadeh, K., Kis, A., Coleman, J. N. & Strano, M. S. Electronics and optoelectronics of two-dimensional transition metal dichalcogenides. *Nature Nanotechnology* **7**, 699–712 (2012). URL http://www.nature.com/nnano/journal/v7/n11/full/nnano.2012.193.html.

13. Pisoni, R. *et al.* Gate-Defined One-Dimensional Channel and Broken Symmetry States in MoS_2 van der Waals Heterostructures. *Nano Letters* **17**, 5008–5011 (2017). URL http://pubs.acs.org/doi/10.1021/acs.nanolett.7b02186.

14. Pisoni, R. *et al.* Gate-tunable quantum dot in a high quality single layer MoS_2 van der Waals heterostructure. *Applied Physics Letters* **112**, 123101 (2018). URL https://aip.scitation.org/doi/10.1063/1.5021113.

15. Bretheau, L. *et al.* Tunnelling spectroscopy of Andreev states in graphene. *Nature Physics* **13** (2017). URL https://www.nature.com/nphys/journal/vaop/ncurrent/full/nphys4110.html.

16. Overweg, H. *et al.* Electrostatically induced quantum point contacts in bilayer graphene. *Nano Letters* **18**, 553–559 (2018). URL https://doi.org/10.1021/acs.nanolett.7b04666.

17. Ando, T., Fowler, A. B. & Stern, F. Electronic properties of two-dimensional systems. *Reviews of Modern Physics* **54**, 437–672 (1982). URL https://link.aps.org/doi/10.1103/RevModPhys.54.437.

18. Isihara, A. & Smrcka, L. Density and magnetic field dependences of the conductivity of two-dimensional electron systems. *Journal of Physics C: Solid State Physics* **19**, 6777 (1986). URL http://stacks.iop.org/0022-3719/19/i=34/a=015.

19. Okamoto, T., Hosoya, K., Kawaji, S. & Yagi, A. Spin Degree of Freedom in a Two-Dimensional Electron Liquid. *Physical Review Letters* **82**, 3875–3878 (1999). URL https://link.aps.org/doi/10.1103/PhysRevLett.82.3875.

20. Shashkin, A. A., Kravchenko, S. V., Dolgopolov, V. T. & Klapwijk, T. M. Indication of the Ferromagnetic Instability in a Dilute Two-Dimensional Electron System. *Physical Review Letters* **87**, 086801 (2001). URL https://link.aps.org/doi/10.1103/PhysRevLett.87.086801.

21. Vakili, K., Shkolnikov, Y. P., Tutuc, E., De Poortere, E. P. & Shayegan, M. Spin Susceptibility of Two-Dimensional Electrons in Narrow AlAs Quantum Wells. *Physical Review Letters* **92**, 226401 (2004). URL https://link.aps.org/doi/10.1103/PhysRevLett.92.226401.

22. Sidler, M. *et al.* Fermi polaron-polaritons in charge-tunable atomically thin semiconductors. *Nature Physics* **13**, 255–261 (2017). URL https://www.nature.com/articles/nphys3949.

23. Poortere, E. P. D., Tutuc, E., Papadakis, S. J. & Shayegan, M. Resistance Spikes at Transitions Between Quantum Hall Ferromagnets. *Science* **290**, 1546–1549 (2000). URL http://science.sciencemag.org/content/290/5496/1546.

24. Jungwirth, T., Shukla, S. P., Smrka, L., Shayegan, M. & MacDonald, A. H. Magnetic Anisotropy in Quantum Hall Ferromagnets. *Physical Review Letters* **81**, 2328–2331 (1998). URL https://link.aps.org/doi/10.1103/PhysRevLett.81.2328.

25. Wang, J. I.-J. *et al.* Electronic Transport of Encapsulated Graphene and WSe_2 Devices Fabricated by Pick-up of Prepatterned hBN. *Nano Letters* **15**, 1898–1903 (2015). URL http://dx.doi.org/10.1021/nl504750f.

Acknowledgements We thank Emanuel Tutuc, Beat Bräm, Ovidiu Cotlet, Matija Karalic and Giorgio Nicolí for fruitful discussions. We thank Peter Märki, Erwin Studer, as well as the FIRST staff for their technical support. We acknowledge financial support from ITN Spin-NANO Marie Sklodowska-Curie grant agreement no. 676108, the Graphene Flagship and the National Center of Competence in Research on

Quantum Science and Technology (NCCR QSIT) funded by the Swiss National Science Foundation. Growth of hexagonal boron nitride crystals was supported by the Elemental Strategy Initiative conducted by the MEXT, Japan and JSPS KAKENHI Grant Numbers JP15K21722.

Author contributions RP fabricated the devices and performed the measurements. RP and AK wrote the manuscript. PB performed the optical characterizations. AK, MB, AI, GB, TI and KE helped to develop the theoretical understanding. ZL, ME, HO, YL and PR supported device fabrication and data analysis. KW and TT provided high-quality Boron-Nitride. GB, TI and KE supervised the work.

Additional information Supplementary information is available. Correspondence and requests for materials should be addressed to R. Pisoni (email: pisonir@phys.ethz.ch) and K. Ensslin (email: ensslin@phys.ethz.ch).

Competing Interests The authors declare that they have no competing financial interests.